Site-selective magnetic order of neptunium in Np_2Ni_{17}

A. Hen,[1,2] N. Magnani,[1] J.-C. Griveau,[1] R. Eloirdi,[1] E. Colineau,[1] J.-P. Sanchez,[3,4] I. Halevy,[2,5] A. L. Kozub,[6,7] A. B. Shick,[6] I. Orion,[2] and R. Caciuffo[1]

[1]*European Commission, Joint Research Centre (JRC), Institute for Transuranium Elements (ITU), Postfach 2340, D-76125 Karlsruhe, Germany*

[2]*Nuclear Engineering Department, Ben Gurion University, Beer-Sheva, Israel*

[3]*CEA, INAC-SPSMS, FR-38000 Grenoble, France*

[4]*Université de Grenoble Alpes, INAC-SPSMS, FR-38000 Grenoble, France*

[5]*Physics Department, Nuclear Research Center Negev, P.O. Box 9001, Beer-Sheva, Israel*

[6]*Institute of Physics, Academy of Sciences of the Czech Republic, Na Slovance 2, CZ-182 21 Prague, Czech Republic*

[7]*Faculty of Applied Physics and Mathematics, Gdansk University of Technology, Narutowicza 11/12, 80-233 Gdansk, Poland*

(Received 10 March 2015; revised manuscript received 11 May 2015; published 13 July 2015)

We present the results obtained by superconducting quantum interference device (SQUID) magnetometry, specific heat, and Mössbauer spectroscopy measurements carried out on Np_2Ni_{17} polycrystalline samples. We show that long-range magnetic order, with a moment $\mu_{(2b)} \sim 2.25\ \mu_B$, occurs below $T_N = 17.5$ K on the Np ($2b$) sites. A nontrivial situation is observed in that the other Np sites ($2d$) do not take part to the order transition and carry only an induced moment of about 0.2 μ_B below T_N. A combined analysis of the different experimental data sets allowed us to determine key parameters associated with the electronic structure of the system. The experimental results are discussed against first-principles electronic structure calculations based on the spin-polarized local spin density approximation plus Hubbard interaction.

DOI: 10.1103/PhysRevB.92.024410 PACS number(s): 75.30.Gw, 71.70.Ch, 75.30.Cr, 76.80.+y

I. INTRODUCTION

The coexistence of magnetic and nonmagnetic atoms of the same element in an ordered compound is unusual and generally associated with unconventional behavior, such as mixed valence in Ce intermetallics [1], spontaneous toroidal order [2], and magnetic instabilities related to topological frustration [3]. A local moment versus singlet formation on the two inequivalent transition-metal sites of the $LuNiO_3$ insulator, triggering a site-selective Mott transition, has been suggested by a combination of density functional and dynamical mean field theory calculations [4]. As a consequence of a symmetry-breaking lattice distortion, the d electrons on half of the Ni ions in $LuNiO_3$ form a singlet with holes on the surrounding oxygen ions, whereas the d electrons on the other Ni site are localized to form a fluctuating moment. An antiferromagnetic ground state involving only half of the titanium sites has been proposed for the $BaTi_2As_2O$ layered pnictide oxide [5]. Neutron diffraction measurements on $TbRu_2Ge_2$ have revealed that frustrated exchange interactions lead to a "mixed" magnetic phase, where non-Kramers Tb ions occupying equivalent crystallographic sites coexist in two distinct states (one nonmagnetic and the other with a finite magnetic moment) [6].

Here, we demonstrate the occurrence of site-selective magnetic order of trivalent neptunium ions in Np_2Ni_{17}, a hexagonal intermetallic compound crystallizing in the $P6_3/mmc$ (D_{6h}) space group with the Th_2Ni_{17}-type structure. The unit cell contains two formula units, with the Np atoms in the $2b$ and $2d$ positions. These two sites are crystallographically inequivalent, with a different nearest-neighbor Ni and Np coordination. In some rare-earth analogs, this gives rise to a difference in the ordered magnetic moment between 10% and 30% [7]. In most cases, however, the inequivalence does not influence the magnetic properties because of crystallographic disorder or the dominance of exchange processes involving the transition-metal sublattice [8–11].

By combining magnetization, Mössbauer and specific heat measurements we have determined the values of the magnetic moments on the two Np sites of Np_2Ni_{17}, and shown that only one of them takes part in the magnetic transition, whilst the other carries only a smaller (roughly one tenth) induced moment. This remarkable difference is explained in terms of the crystal field potential acting on the two sites, which stabilizes a magnetic doublet on the $2b$ and a nonmagnetic singlet on the $2d$ position.

II. EXPERIMENTAL DETAILS AND RESULTS

Due to the contamination risk generated by the radiotoxicity of the neptunium element, all operations of preparation and encapsulation have been carried out in shielded gloveboxes under inert nitrogen atmosphere following well-established safety procedures. Polycrystalline samples of Np_2Ni_{17} were prepared by arc melting stoichiometric amounts of high-purity elemental constituents (99.9 % Np, 99.996 % Ni) on a water-cooled copper hearth, under Ar (6N) atmosphere. A Zr alloy was used as an oxygen getter. The sample was melted several times and crushed before the last melt, to ensure complete homogeneity of the alloy button. The material was wrapped in a tantalum foil and annealed under dynamic high vacuum at 1423 K for 8 hours and cooled down at 50 K/h to remove a secondary $NpNi_5$ phase.

Published by the American Physical Society under the terms of the Creative Commons Attribution 3.0 License. Further distribution of this work must maintain attribution to the author(s) and the published article's title, journal citation, and DOI.

TABLE I. Fractional atomic coordinates of Np and Ni atoms in the Np_2Ni_{17} unit cell (space group $P6_3/mmc$), as obtained from a Rietveld refinement of the x-ray diffraction profile ($R_{wp} = 0.11$).

Atom	Wyckoff site	x	y	z
Np1	$2b$	0	0	1/4
Np2	$2d$	1/3	2/3	3/4
Ni1	$4f$	1/3	2/3	0.8904(3)
Ni2	$6g$	1/2	0	0
Ni3	$12j$	0.3707(3)	0.0428(4)	1/4
Ni4	$12k$	0.1655(3)	0.3310(8)	0.0185(9)

Powder x-ray diffraction in reflection mode was used to characterize the crystallographic structure at room temperature. Data were collected on a Bruker D8 diffractometer installed inside a shielded glove-box, using Cu-Kα_1 radiation ($\lambda = 0.154\,06$ nm) selected by a Ge (111) monochromator. A 1D position sensitive detector covered the angular range from 15 to 120 degrees, with incremental steps of 0.0085 degrees. The Rietveld analysis of the measured diffraction pattern, performed with the X'PERT HIGHSCORE PLUS software package of PANalytical, shows that the sample is single phase, with a small amount of elemental nickel (~5 wt%) and NpO_2 (~0.8 wt%) impurities. The observed Bragg peaks can be indexed in the hexagonal $P6_3/mmc$ space group, and confirm the Th_2Ni_{17}-type hexagonal structure with lattice parameters $a = 8.282\,15(7)$ Å and $c = 8.040\,29(8)$ Å [12]. Np atoms occupy two distinct crystallographic positions ($2b$ and $2d$), whereas the Ni ones are distributed amongst the $4f$, $6g$, $12k$, and $12j$ positions. The refined atomic fractional coordinates are given in Table I.

As shown in Fig. 1 the two Np sites have a different Np-Np coordination, which makes them magnetically inequivalent. Indeed, although the Np-Np coordination in the a-b plane is the same for both sites (three Np neighbors at 4.781 Å arranged in a equilateral triangle), the $2b$ sites also form 1-D chains along the c axis, whereas for the $2d$ sites these chains are interrupted by the Ni $4f$ sites. The $2b$ intrachain distance of $c/2 = 4.020$ Å is the smallest Np-Np distance in this compound, and is much larger than the so-called Hill limit of ~3.2 Å that separates Np compounds with localized $5f$ states from itinerant systems. The hybridization between $5f$ states and conduction electrons should therefore be limited and appreciable crystal field effects are expected, in a scenario similar to the one observed for analog rare-earth intermetallic compounds.

A MPMS-7 SQUID and a PPMS-14T from Quantum Design (QD) were used for dc magnetic characterization in the temperature range 1.9–300 K, with an external magnetic field up to 14 T. The temperature (T) dependence of the magnetic susceptibility $\chi(T)$ (approximately evaluated as $M(T)/H$ and measured in a field $B = \mu_0 H = 7$ T) is shown in Fig. 2. The difference between the susceptibility curves recorded after zero-field and field-cooling conditions were smaller than the experimental uncertainties. Data have been corrected for the presence of a ferromagnetic impurity equivalent to ~3 wt% of elemental nickel, in good agreement with the Ni content estimated by x-ray diffraction. A weak anomaly at $T_N \simeq 17.5$ K reveals the onset of long-range magnetic order. Above ~70 K, the magnetic susceptibility exhibits a Curie-Weiss

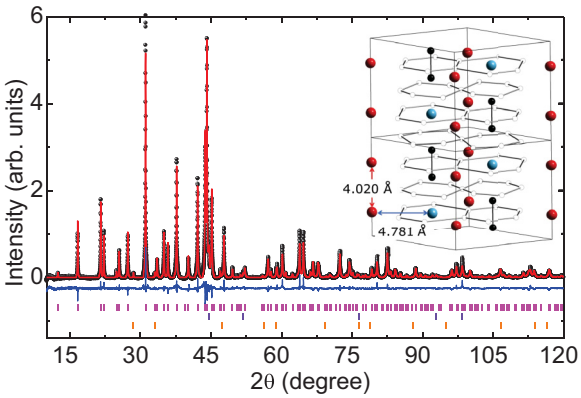

FIG. 1. (Color online) X-ray diffraction pattern recorded for Np_2Ni_{17} at room temperature; dots are experimental data and the solid red line is the calculated Rietveld profile, the residual being represented by the blue line at the bottom. Ticks represent the expected angular position of Bragg peaks: top row Np_2Ni_{17}, middle row elemental Ni impurity (~5 wt%), bottom row NpO_2 impurity (~0.8 wt%). (Inset) Crystallographic unit cell of Np_2Ni_{17} (Space Group $P6_3/mmc$). Np atoms at the $2b$ ($2d$) Wyckoff position are represented by red (blue) large spheres; Ni atoms located at the $4f$ positions are represented by small black spheres, all the other Ni atoms by small open circles. The shortest Np-Np interatomic distances are indicated by arrows.

behavior with a molar Curie constant $C = 9.7$ emu K mol^{-1} and a Curie-Weiss temperature $\theta_{CW} = -41$ K. Assuming an effective paramagnetic moment for the trivalent (see below, Mössbauer) Np ions $\mu_{eff}^{Np} = 2.88\ \mu_B$, corresponding to the intermediate coupling free-ion value, one obtains $\mu_{eff}^{Ni} = 1.89\ \mu_B$ per Ni atom, in line with previously reported estimates for R_2Ni_{17} rare-earth (R) analogs [13]. The negative value of θ_{CW} indicates the presence of antiferromagnetic interactions, probably leading to a ferrimagnetic ground state as observed for several heavy rare-earth R_2Ni_{17} compounds [7]. This is in contrast with Np_2Co_{17}, which is a ferromagnet and behaves

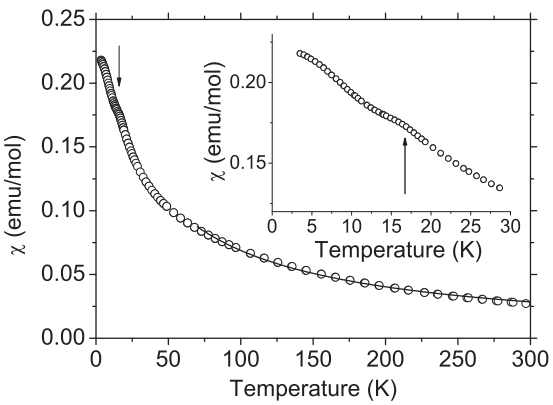

FIG. 2. Temperature dependence of the magnetic susceptibility measured on a polycrystalline sample of Np_2Ni_{17} between 2 and 300 K after zero-field cooling in a field $B = 7$ T. The solid line is a fit to the Curie-Weiss law above 70 K. The arrow indicates the anomaly corresponding to a magnetic transition at 17.5 K. The inset shows the low-temperature region on an enlarged scale.

MOST WIEDZY Downloaded from mostwiedzy.pl

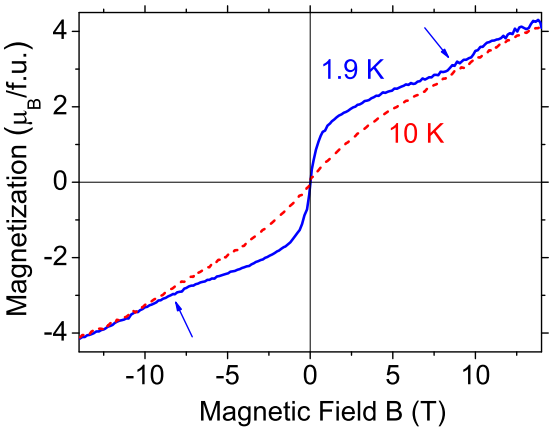

FIG. 3. (Color online) Magnetization curves of Np_2Ni_{17} measured up to 14 T at 10 (dashed line) and 1.9 K (solid line).

like light rare-earth R_2Ni_{17} compounds. As shown in Fig. 3, the magnetization cycle does not show hysteresis and a magnetic field of 14 T is not sufficient to saturate the sample, even at the lowest studied temperature of 1.9 K. The variation of the slope of the magnetization curve observed at about 8 T could indicate a rearrangement of the spin directions in the Ni sublattice as suggested for Y_2Ni_{17} [14].

The ^{237}Np Mössbauer measurements [15] were performed in transmission geometry on a powder absorber with a thickness of ∼140 mg cm^{-2} of Np. The Mössbauer source (∼108 mCi of ^{241}Am metal) was kept at 4.2 K, while the temperature of the absorber was varied from 4.2 to 55 K in discrete steps. The spectra were recorded with a sinusoidal drive system using conventional methods. The velocity scale was calibrated with reference to a $NpAl_2$ standard (B_{hf} = 330 T at 4.2 K). The recorded spectra are shown in Fig. 4.

The temperature evolution of the Mössbauer spectra reveals the occurrence of a magnetic phase transition below 18 K, with a fully split hyperfine pattern suggesting the stabilization of long-range magnetic order at low temperature. Solid lines in Fig. 4 are fits of the spectra obtained by solving the complete Hamiltonian for the hyperfine interactions and assuming a Lorentzian shape for the absorption lines, including relaxation broadening (in the ordered state). The main component of the electric field gradient ($eq \equiv V_{zz}$) is taken collinear with the hyperfine field B_{hf}, i.e., along the crystal c axis, and the asymmetry parameter (η) is set to zero, as imposed by the axial symmetry of the Np sites.

In the paramagnetic phase, the poorly resolved spectra are accounted for by assuming the presence of two inequivalent Np sites (1 : 1) with different isomer shift [$\delta_{IS}(2b) \sim -12.8(5)$ mm/s and $\delta_{IS}(2d) \sim -14.0(5)$ mm/s with reference to $NpAl_2$; quadrupole coupling constant $|e^2qQ_{(2b)}| \sim 23.5(1)$ mm/s and $|e^2qQ_{(2d)}| \sim 11.3(1)$ mm/s] corresponding to the 2b and 2d crystallographic sites. The observed isomer shifts are compatible with a $5f^4$ trivalent state of Np ions in a metallic compound [16]. As shown in Fig. 5, a good fit of the data at 4.2 K in the ordered phase required two different sets of hyperfine parameters. We find $e^2qQ_{(2b)} \sim +17.6(3)$ mm/s, whereas $e^2qQ_{(2d)} \sim -2.0(5)$ mm/s. The 2b site carries a large moment [$\mu_{(2b)} = 2.25\ \mu_B$], the other being only weakly magnetic [$\mu_{(2d)} \sim 0.2\ \mu_B$], as inferred from the respective values

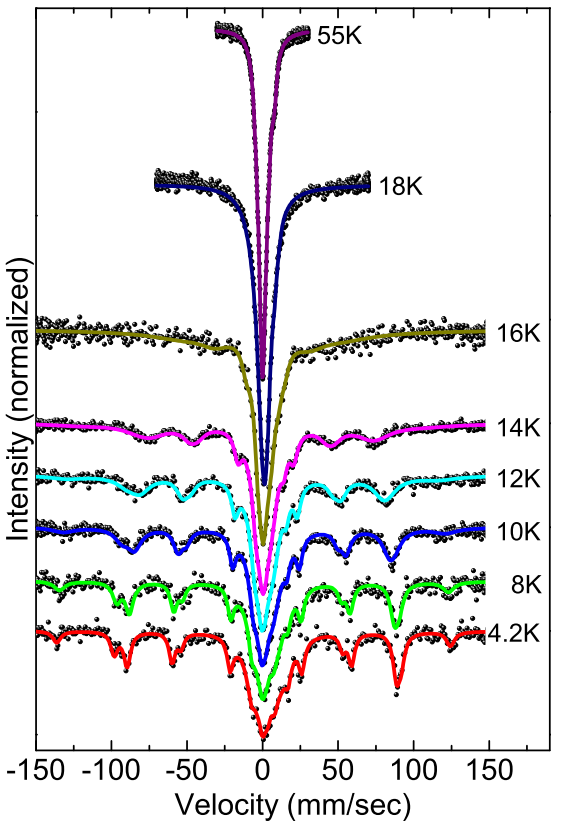

FIG. 4. (Color online) Temperature evolution of the Mössbauer spectra measured for Np_2Ni_{17}. Dots are measured data, solid lines are the results of the fit to the model described in the text.

of the hyperfine field [B_{hf} = 483(1) and 40(2) T, respectively] using the relation $B_{hf}/\mu_{Np} = 215 \pm 5$ T/μ_B [17]. This is consistent with the crystallographic structure of the compound, although in many rare-earth isostructural analogs with Co and Fe, as well as in Np_2Co_{17} [17], the difference between the two sites is washed out by the prevalence of the molecular field [10] and by some degree of crystallographic disorder [8,9].

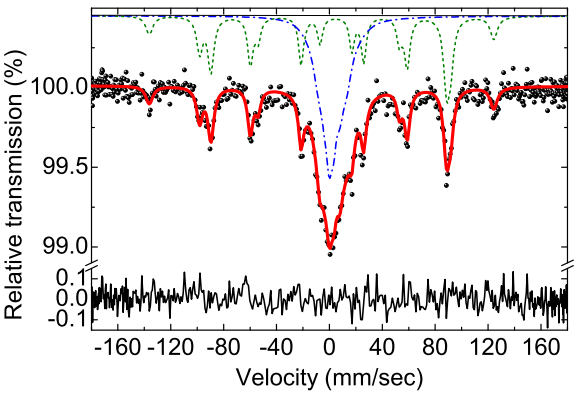

FIG. 5. (Color online) The Mössbauer spectra measured for Np_2Ni_{17} at 4 K. Dots are measured data, the solid line is the results of a fit assuming that the 2b (green dashed line) and the 2d (blue dash-dotted line) sites are respectively strongly and weakly magnetic. The difference between calculated curve and experimental data is shown at the bottom of the plot.

MOST WIEDZY Downloaded from mostwiedzy.pl

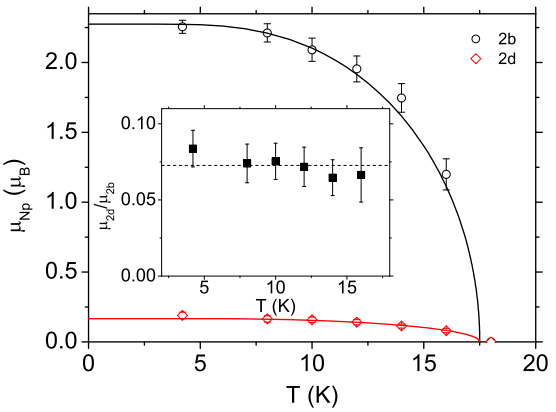

FIG. 6. (Color online) Ordered magnetic moment on the Np 2*b* (black open circles) and the Np 2*d* (red closed circles) sites. Solid lines are calculated by a mean-field model described in the text. The temperature dependence of the ratio between the magnetic moment on the two Np sites is shown in the inset.

The temperature dependence of the ordered magnetic moment has been obtained from the variation of the hyperfine field and is shown in Fig. 6. The observed continuous decrease of the order parameter is compatible with a second-order phase transition. The absence of hysteresis in the magnetic and specific heat measurements, as well as their shape, support this conclusion. Saturating the Np moments in the ordered phase would give a contribution to the magnetization of 2.4 μ_B per formula unit, a value significantly smaller than that measured at 1.9 K with an applied field of 14 T. This means that the Ni sublattice carries an ordered magnetic moment of at least 0.1 μ_B per Ni atom; values of similar order of magnitude have been reported for several rare-earth analogs [7].

The solid lines in Fig. 6 are fits of the data to a $J = 1/2$ Brillouin function, as expected for a molecular field mainly associated with the Ni sublattice. The fact that the ratio between the ordered moment on the two inequivalent Np sites is temperature independent suggests that the same molecular field acts on both sites. On the other hand, the large difference in magnitude between the two moments reflects their different anisotropy. As shown in Table II, this behavior can be qualitatively reproduced by a simple crystal field model. The CF Hamiltonian appropriate for the D_{6h} symmetry of the Np sites is

$$H_{CF} = B_2^0 O_2^0 + B_4^0 O_4^0 + B_6^0 O_6^0 + B_6^6 O_6^6, \qquad (1)$$

TABLE II. Crystal-field energy spectra in the paramagnetic phase calculated for the inequivalent 2*b* and 2*d* sites of Np^{3+} in Np_2Ni_{17}.

Np_1 (2*b*)		Np_2 (2*d*)	
Energy (cm^{-1})	Symmetry	Energy (cm^{-1})	Symmetry
0	$\Gamma_5^{(1)}$	0	Γ_4
6	Γ_4	264	$\Gamma_5^{(1)}$
109	Γ_1	550	Γ_1
358	Γ_6	566	Γ_6
626	Γ_3	620	Γ_3
750	$\Gamma_5^{(2)}$	734	$\Gamma_5^{(2)}$

where O_k^q are Stevens operator equivalents. Reasonable values of the B_k^q parameters can be obtained by rescaling those determined for the isostructural Er_2Ni_{17} compound [18]. Taking into account the different radial extension of the $5f$ and $4f$ wave functions [19,20] and the different Stevens coefficients [21], we obtain for site 2*b* $B_2^0 = -5.77$ cm^{-1}, $B_4^0 = -0.144$ cm^{-1}, $B_6^0 = 7.14 \times 10^{-3}$ cm^{-1}, $B_6^6 = 0.123$ cm^{-1}, leading to a $\Gamma_5^{(1)} = 0.943|\pm 4\rangle - 0.331|\mp 2\rangle$ doublet ground state, followed by a low-lying $\Gamma_4 = (|3\rangle - |-3\rangle)/\sqrt{2}$ singlet at about 6 cm^{-1}. For the 2*d* site, the CF parameters are $B_2^0 = -2.55$ cm^{-1}, $B_4^0 = 0.077$ cm^{-1}, $B_6^0 = 2.46 \times 10^{-3}$ cm^{-1}, $B_6^6 = 0.123\,cm^{-1}$. The opposite sign of B_4^0 leads to a Γ_4 ground state separated by more than 250 cm^{-1} from the first excited state ($\Gamma_5^{(1)}$). An exchange contribution $2\mu_B(g_J - 1)H_{ex}J_z$ to the Hamiltonian, where we assume that the exchange field H_{ex} is oriented along the *c* axis, leads to an ordered moment along *c* on the 2*b* site. On the other hand, the singlet ground state for the 2*d* site has no intrinsic ordered moment, but a small moment can be induced by the molecular field through mixing with the excited Γ_3 level at about 620 cm^{-1}. For $H_{ex} = 21$ T, one obtains $\mu_{(2d)} = 0.19\,\mu_B$ and $\mu_{(2b)} = 2.21\,\mu_B$, in agreement with the experiment.

The above crystal field and exchange model can be used to evaluate the different contributions to the electric field gradient observed at the 2*b* site at 4.2 K. At this temperature, the $\Gamma_5^{(1)}$ doublet is split by the molecular field and its lowest level $0.951|+4\rangle - 0.309|-2\rangle$, which lies about 31 K below the Γ_4 singlet, is essentially the only one populated. The electronic $5f$ contribution to the quadrupole coupling constant is proportional to $\langle 3J_z^2 - J(J+1)\rangle \approx 24.6$. For the free ion Np^{3+}, $\langle 3J_z^2 - J(J+1)\rangle = 28$ and the quadrupole coupling constant due to the $5f$ electrons amounts to -27.3 mm/s [17]. It follows that $e^2q^{5f}Q_{(2b)} = -23.9$ mm/s. From the experimental value, $e^2q^{5f}Q_{(2b)} + e^2q^{latt}Q_{(2b)} = +17.6$ mm/s, we conclude that the sum of lattice and electron contributions ($e^2q^{latt}Q$) amounts to 41.5 mm/s, i.e., $V_{zz}^{latt}(2b) = 2 \times 18$ V/cm^2 using the value of 4.1×10^{-24} cm^2 for the quadrupole moment of the ^{237}Np ground state.

A QD PPMS-14 platform equipped with a closed-cycle ^{3}He probe was used to carry out specific heat measurements. Thanks to the relatively low self-heating effect of ^{237}Np ($W = 2.03$ μW/g) we have been able to collect data down to 0.5 K using a 1.2-mg sample. To prevent external contamination, the sample was encapsulated in Stycast® 2850 FT epoxy resin, whose contribution to the measured heat capacity was subtracted according to a standard procedure. The results are shown in Fig. 7. A clear lambda-type anomaly is observed at the transition temperature $T_N = 17.5$ K. The vibrational contribution has been estimated from specific heat measurements performed on $ThNi_5$ (a compound with a closely related crystallographic structure), subtracting the electronic term as detailed in Ref. [22] and rescaling to account for the different number of atoms in the unit cell. At lower temperatures, Schottky peaks of nuclear and electronic origin contribute to the observed temperature dependence (lower inset in Fig. 7). The latter has been fitted by a Schottky anomaly corresponding to two electronic levels split by 5 K. The former has been described by the Hamiltonian $-g_I\mu_N B_{hf} I_z$, where $I = 5/2$ is the nuclear angular moment of ^{237}Np, I_z its component along the

MOST WIEDZY Downloaded from mostwiedzy.pl

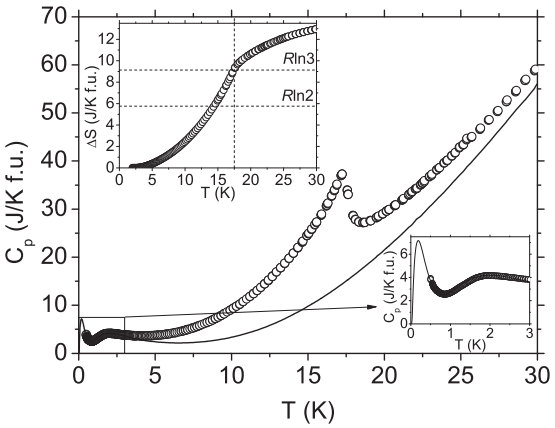

FIG. 7. Temperature dependence of the specific heat measured for Np_2Ni_{17} between 0.5 and 30 K. The solid line is the estimated sum of the vibrational, nuclear, and electronic Schottky contributions. The inset shows the magnetic entropy difference $\Delta S = S(T) - S(2\ \mathrm{K})$ calculated by integrating the C_p/T curve after subtracting the nonmagnetic contributions.

quantization axis, μ_N is the nuclear magneton, g_I the g-factor, and the value of the hyperfine field $B_{hf} = 483$ T was estimated by Mössbauer spectroscopy. The nuclear ground multiplet on the Np $2b$ site is split into six levels equally separated by 0.22 K.

The magnetic entropy released at the phase transition is shown in the inset of Fig. 7, and is close to $R\ln 3$ at T_N. This value confirms that only one Np site has a doublet ground state (otherwise the contribution from both sites would be at least $R\ln 4$) and that a sizable Ni contribution is present.

III. ELECTRONIC-STRUCTURE CALCULATIONS

To examine theoretically the electronic structure of Np_2Ni_{17} and to make a comparison with the experimental data, we performed spin-polarized local spin density approximation (LSDA) as well as LSDA plus Hubbard U (LSDA+U) calculations, using the experimental lattice parameters for the Th_2Ni_{17}-type structure (see Table III). All calculations are performed with the in-house implementation [23,24] of the full-potential linearized augmented plane wave (FP-LAPW) method [25]. This FP-LAPW version includes all relativistic effects: scalar-relativistic and spin-orbit coupling (SOC). The radii of the atomic muffin-tin (MT) spheres are set to 2.80 a.u. (Np) and 2.05 a.u. (Ni). The basis set size is characterized by the parameter $R_{\mathrm{Np}} \times K_{\max} = 8.4$ and the Brillouin zone is sampled with 425 k points.

TABLE III. Spin (μ_S), orbital (μ_L), and total ($\mu = \mu_S + \mu_L$) magnetic moments in the muffin-tin spheres around Np and Ni atoms (in μ_B units), together with total values (including the interstitial spin moment contribution) per formula unit (f.u.) of μ_S, μ_L, and μ.

		LSDA(+SOC)			AMF-LSDA+U			
Atom	Site	μ_S	μ_L	μ	μ_S	μ_L	μ	μ (exp)
Np_1	$2b$	−2.80	2.99	0.19	−1.46	3.92	2.46	2.25
Np_2	$2d$	2.58	−3.53	−0.95	0.43	−0.26	0.17	0.2
Ni_1	$4f$	0.11	0.01	0.12	0.28	0.03	0.31	>0.1[a]
Ni_2	$6g$	0.24	0.04	0.28	0.33	0.03	0.36	>0.1[a]
Ni_3	$12j$	0.20	0.02	0.22	0.27	0.03	0.30	>0.1[a]
Ni_4	$12k$	0.27	0.01	0.28	0.29	0.02	0.31	>0.1[a]
Total		3.35	−0.22	3.13	3.62	4.11	7.73	>4.1[b]

[a]Value averaged over all Ni sites.

[b]Only a lower boundary can be given because the magnetization is not saturated at the largest available magnetic field (14 T).

First, we apply the conventional spin-polarized LSDA, initiating the spin polarization at Np ($2b$) atoms in the unit cell. In these calculations the magnetization is aligned along the z axis (out-of-plane). Table III reports the calculated spin (μ_S), orbital (μ_L), and total ($\mu = \mu_S + \mu_L$) magnetic moments in the MT spheres around Np and Ni atoms (in μ_B units), together with the total values per formula unit (f.u.) (including the spin moment contribution from the interstitial region). We observe an antiparallel coupling between Ni-$3d$ and $5f$ spin moments on the ($2b$) site, according to the mechanism proposed in Ref. [26]. The Np atoms on the two sites have spin moments of opposite sign and about the same magnitude. The angular component of the total moment is antiparallel to the spin-only contribution as it is expected for a less-than-half-filled f shell.

Next, we apply LSDA+U calculations, making use of relativistic (including SOC) "around-mean-field" (AMF)-LSDA+U [27]. The Coulomb interaction in the Np $5f$ shell is parameterized by Slater integrals $F_0 = 3.00$ eV, $F_2 = 7.43$ eV, $F_4 = 4.83$ eV, and $F_6 = 3.53$ eV, as given in Ref. [28]. They correspond to commonly accepted values $U = 3$ eV and $J = 0.6$ eV for the Coulomb and exchange interactions parameters, respectively.

The total electron-energy density of states (DOS) calculated for $U = 3$ eV is shown in Fig. 8, together with the spin-resolved d-orbital projected DOS for Ni atoms at the occupied lattice sites, and the f-orbital projected DOS for Np atoms. The Ni-$d^{\uparrow}$ band is practically full, whereas the Ni-$d^{\downarrow}$ band is partially occupied. Note the similarity between the Np ($2b$) f-projected DOS shown in Fig. 8(c) and the DOS for Np ($1a$) atom in $NpNi_5$ [22].

Clearly, first-principles calculations correctly predict the presence of two magnetically inequivalent Np sites. Moreover, when the LSDA+U approximation is applied, the calculated magnetic moments are in good quantitative agreement with the experiment. However, it must be noted that the AMF-LSDA+U solution shown in Table III is obtained initiating the spin polarization at Np ($2b$) atoms. When the initial occupation matrices are chosen after the spin-polarised LSDA, another self-consistent AMF-LSDA+U solution is obtained. In this case, for the Np ($2b$) we obtain the spin $\mu_S = -1.78\ \mu_B$, orbital $\mu_L = 3.98\ \mu_B$, and total $\mu = \mu_S + \mu_L = 2.20\ \mu_B$ magnetic moments in a reasonable agreement with the experimental data. For the Np ($2d$), the spin $\mu_S = 1.98\ \mu_B$, orbital $\mu_L = -4.07\ \mu_B$, and total $\mu = -2.09\ \mu_B$ magnetic moments are calculated. This relatively large magnitude of μ exceeds substantially the experimental value. The magnetic character of the Ni atoms remains very similar to that shown in Table III. Note that the occurrence of multiple solutions (local minima) is a rather common feature of the LSDA+U method, and is well documented in the literature [29,30]. It constitutes one of the limitations of the static mean-field LSDA+U

MOST WIEDZY Downloaded from mostwiedzy.pl

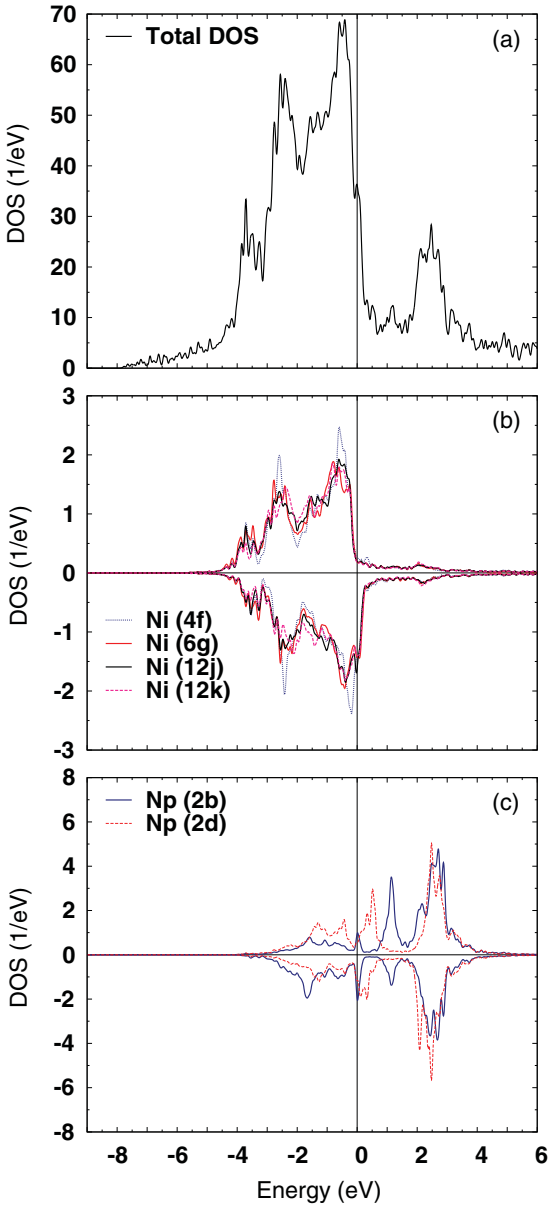

FIG. 8. (Color online) (a) The total electron-energy density of states (DOS) per formula units for Np_2Ni_{17} calculated with relativistic LSDA+U ($U = 3$ eV); (b) the d-orbital projected DOS for Ni atoms at $4f$,$6g$, $12j$, and $12k$ special positions of the $P6_3/mmc$ space group; (c) the f-orbital projected DOS for Np atoms at $2b$ and $2d$ positions.

approximation due to the use of a single particle Hilbert space. A more careful investigation that takes into account a configurational interaction is needed to better understand the magnetic behavior in Np_2Ni_{17}.

IV. CONCLUSIONS

^{237}Np Mössbauer spectra have been measured on Np_2Ni_{17} and revealed the presence of two strongly inequivalent Np sublattices, at variance with widely studied rare earth and actinide isostructural analogs. In the magnetically ordered phase below $T_N = 17.5$ K, the Mössbauer absorption spectra are indeed given by the sum of two components with equal total weight, one fully splitted and corresponding to a large value of the hyperfine field [$B_{hf} = 483(1)$ T], the other showing a broad central absorption line indicating the presence of a second Np site on which the hyperfine field is one order of magnitude smaller [$B_{hf} = 40(2)$ T]. This result clearly demonstrates that the two Np crystallographic sites ($2b$ and $2d$) are magnetically inequivalent, with ordered moment of $\sim$2.25 μ_B and $\sim$0.2 μ_B, respectively. Such a conclusion is corroborated by the variation of the magnetic entropy near the transition temperature, which confirms that only half of the Np atoms in the lattice takes part in the magnetic transition. On the other hand, magnetic susceptibility measurements suggest that the magnetic behavior of the nickel sublattice in Np_2Ni_{17} is very similar to that exhibited by rare-earth analogs, both in the ordered and in the paramagnetic phase. A simple crystal field model with localized $5f$ electrons is sufficient to explain this uncommon behavior. The crystal field approach is justified by the large Np-Np nearest neighbor distance, which is about 25% larger than the empirical limit separating delocalized $5f$ electronic states from localized ones in Np compounds. The fact that the fourth-order axial crystal field potential has opposite sign on the two Np sites, has qualitatively important consequences as the singlet-doublet sequence of the two lowest energy levels is reverted. This makes one Np site magnetic, whereas the second carries only a magnetic moment induced by the molecular field. The physical picture revealed by the experiment is also supported by first-principle calculations based on the LSDA+U approximation with around mean-field double-counting corrections. We have shown that using this calculation approach it is possible to describe the magnetism on the Ni sublattice and reproduce the large difference between the magnetic moments carried out by the two Np sites.

ACKNOWLEDGMENTS

We thank D. Bouëxière, G. Pagliosa, and P. Amador Celdran, for their technical support. The high-purity neptunium metal required for the fabrication of the sample was made available through a loan agreement between Lawrence Livermore National Laboratory and ITU, in the frame of a collaboration involving LLNL, Los Alamos National Laboratory, and the U.S. Department of Energy. A.H. acknowledges the European Commission for support in the frame of the Training and Mobility of Researchers programme. The support from the Czech Science Foundation (GACR) Grant No. 15-07172S is acknowledged.

[1] K. Prokeš, S. Hartwig, A. Gukasov, J. A. Mydosh, Y.-K. Huang, O. Niehaus, and R. Pöttgen, Phys. Rev. B **91**, 014424 (2015).

[2] S. Hayami, H. Kusunose, and Y. Motome, Phys. Rev. B **90**, 024432 (2014).

[3] S. Giri, H. Nakamura, and M. Shiga, Phys. Rev. B **59**, 13943 (1999).

[4] H. Park, A. J. Millis, and C. A. Marianetti, Phys. Rev. Lett. **109**, 156402 (2012).

MOST WIEDZY Downloaded from mostwiedzy.pl

[5] X.-L. Yu, D.-Y. Liu, Y.-M. Quan, T. Jia, H.-Q. Lin, and L.-J. Zou, J. Appl. Phys. **115**, 17A924 (2014).
[6] A. Garnier, D. Gignoux, D. Schmitt, and T. Shigeoka, Phys. Rev. B **57**, 5235 (1998).
[7] O. Moze, J. M. Cadogan, S. J. Kennedy, and K. H. J. Buschow, Physica B **319**, 35 (2002).
[8] K. Clausen and B. Lebech, J. Phys. C Solid State **15**, 5095 (1982).
[9] P. C. M. Gubbens and K. H. J. Buschow, J. Phys. F Met. Phys. **12**, 2715 (1982).
[10] M. D. Kuz'min, Y. Skourski, K. P. Skokov, and K.-H. Müller, Phys. Rev. B **75**, 184439 (2007).
[11] O. Moze, R. Caciuffo, B. Gillon, G. Calestani, F. E. Kayzel, and J. J. M. Franse, Phys. Rev. B **50**, 9293 (1994).
[12] M. Akabori, R. G. Haire, J. K. Gibson, Y. Okamoto, and T. Ogawa, J. Nucl. Mater. **247**, 240 (1997).
[13] I. Pop, M. Andrecut, and I. Burda, J. Phys. D: Appl. Phys. **26**, 1445 (1993).
[14] M. Coldea and I. Pop, in *The Rare Earths in Modern Science and Technology*, edited by G. J. McCarthy, H. B. Silber, and J. J. Rhyne (Plenum Press, New York, 1982), Vol. 3, pp. 407–412.
[15] E. Colineau, P. Gaczyński, J.-C. Griveau, R. Eloirdi, and R. Caciuffo, Hyperfine Interact. **207**, 113 (2012).
[16] J. P. Sanchez, D. Aoki, R. Eloirdi, P. Gaczyński, J.-C. Griveau, E. Colineau, and R. Caciuffo, J. Phys-Condens. Mat. **23**, 295601 (2011).
[17] I. Halevy, A. Hen, I. Orion, E. Colineau, R. Eloirdi, J.-C. Griveau, P. Gaczyński, F. Wilhelm, A. Rogalev, J.-P. Sanchez, M. L. Winterrose, N. Magnani, A. B. Shick, and R. Caciuffo, Phys. Rev. B **85**, 014434 (2012).
[18] P. C. M. Gubbens, A. A. Moolenaar, G. A. Stewart, F. M. Mulder, and K. H. J. Buschow, J. Magn. Magn. Mater. **140-144**, 1011 (1995).
[19] J. Desclaux and A. Freeman, J. Magn. Magn. Mater. **8**, 119 (1978).
[20] A. Freeman and J. Desclaux, J. Magn. Magn. Mater. **12**, 11 (1979).
[21] G. Amoretti, J. Physique **45**, 1067 (1984).
[22] A. Hen, E. Colineau, R. Eloirdi, J.-C. Griveau, N. Magnani, F. Wilhelm, A. Rogalev, J.-P. Sanchez, A. B. Shick, I. Halevy, I. Orion, and R. Caciuffo, Phys. Rev. B **90**, 054408 (2014).
[23] A. B. Shick, D. L. Novikov, and A. J. Freeman, Phys. Rev. B **56**, R14259(R) (1997).
[24] A. B. Shick and W. E. Pickett, Phys. Rev. Lett. **86**, 300 (2001).
[25] E. Wimmer, H. Krakauer, M. Weinert, and A. J. Freeman, Phys. Rev. B **24**, 864 (1981).
[26] M. Brooks, O. Eriksson, and B. Johansson, J. Phys-Condens. Mat. **1**, 5861 (1989).
[27] A. B. Shick, V. Drchal, and L. Havela, Europhys. Lett. **69**, 588 (2005).
[28] K. T. Moore and G. van der Laan, Rev. Mod. Phys. **81**, 235 (2009).
[29] B. Dorado, B. Amadon, M. Freyss, and M. Bertolus, Phys. Rev. B **79**, 235125 (2009).
[30] Note that in the LSDA + U method, which is used for our calculations, the total energy functional depends not only on the charge/spin densities, but also on the individual on-site occupations of the f shell. The total energy functional is then minimized in the single-particle Hilbert space (the same used in DFT-LSDA/GGA calculations). Starting from different initial guesses for the f-shell occupation, the self-consistent solution converges to the different local minima rather than to the true ground state as in the DFT (LSDA/GGA).

MOST WIEDZY Downloaded from mostwiedzy.pl